Kinetic investigation and numerical modelling of $CaCO_3/Al_2O_3$ reactor for high-temperature thermal energy storage application.

Arun Mathew [a,*], Nima Nadim [a], Tilak. T. Chandratilleke [a],
Mark Paskevicius [b], Terry D. Humphries [b], Craig E. Buckley [b]

[a] School of Civil and Mechanical Engineering, Curtin University
Curtin University, GPO Box U1987, Perth, WA 6845, Australia

[b] Department of Physics and Astronomy, Curtin University, GPO Box U1987, Perth, WA 6845, Australia

Abstract

This study conducts kinetic analyses of the carbonation reaction of $CaCO_3$ (doped with Al_2O_3) as well as parametric analyses of the performance of a thermochemical reactor, which can act as a thermal battery. Kinetic measurements of CO_2 release and absorption were carried out using thermogravimetric analysis (TGA) at 815, 830 and 845 °C on a $CaCO_3/Al_2O_3$ sample that had been previously cycled over 500 times. The rapid reaction kinetics revealed that the Avrami nucleation growth model with exponent 3 fits well to explain the carbonation reaction. The numerical study considered a cylindrical reactor with a height and diameter of 100 mm. According to numerical analysis, at an applied CO_2 pressure of 1 bar, increasing the thermal conductivity of the reactor bed from 1.33 to 5 W/m.K increases the rate of carbonation reaction by 74 %. When the applied CO_2 pressure is increased from 1 to 2 bar, the performance of the reactor bed with thermal conductivity of 1.33 W/m.K improves by 42%; however, when the applied CO_2 pressure is increased from 2 to 3 bar, the performance improves by only 18%. Additionally, when the boundary temperature of the reactor was lowered by 30 °C, performance was enhanced by 43% at an applied CO_2 pressure of 1 bar. This study also examined the effect of using a graphite fin as a heat extraction system. The graphite fin allowed for more rapid heat extraction and increased the carbonation reaction by 44% in the reactor bed with poor thermal conductivity (1.33 W/m.K) but had no effect in the reactor with modest thermal conductivity of (5 W/m.K) due to its ability to already transfer heat effectively to the

* Corresponding author.
E-mail address: arun.mathew@postgrad.curtin.edu.au (Arun Mathew)

reactor shell. The study demonstrates some of the limitations of poor thermal transport in a thermochemical battery.

Nomenclature			
Symbols			
C_P	specific heat capacity, J/kg.K	t	time, s
E_a	activation energy, J/mol	ρ	density, kg/m^3
ΔH	molar enthalpy of reaction, J/mol	ε	porosity
k	kinetic coefficient, 1/s	dx/dt	carbonation velocity, 1/s
k_0	pre-exponential factor, 1/s	λ	thermal conductivity, W/m.K
M	molar mass of CO_2, kg/mol	**Subscript**	
$\dot{Q}$	heat source, W/m^3	s	Solid reactant
P	CO_2 pressure, Pa	eq	equilibrium
ΔS	reaction entropy, J/ mol. K	gas	gas, CO_2
R	universal gas constant, J/mol. K	e	effective
T	temperature, K	ref	reference
λ	thermal conductivity, W/m.K	ini	initial
wt	maximum mass content of CO_2, %	app	applied

Introduction

The transition of energy harnessing from non-renewable to renewable energy is inexorable in the coming decades due to the environmental impact and limited availability of fossil fuels. A great technological challenge surrounds the storage of energy that can be generated by the raft of emerging renewables to provide base-load power. A thermal energy storage (TES) system integrated with concentrated solar plants (CSP) can effectively counter the intermittency issue and provide a continuous energy supply. Compared to energy storage in batteries, the low cost and ease of integration of TES into large facilities are significant advantages of CSP over other technologies [1, 2]. According to the energy storage technique used, TES can be classified as sensible, latent, or thermochemical. Among the three options, thermochemical energy storage's superior characteristics such as higher energy density, the potential to be a low-cost system, and theoretically infinite energy storage duration have made it an appealing option [3, 4]. However, thermochemical energy storage remains a laboratory-scale endeavour due to the complexities associated with its more complicated reactions and overall system complexity [5, 6].

One of the critical requirements for developing a successful thermochemical energy storage system is the development of an appropriate energy storage material. A prospective storage material should possess the necessary chemical, thermophysical, and economic properties. Numerous materials have been considered in these aspects, including metal hydrides, hydroxides, oxides and carbonates [7]. Among the energy storage materials available, calcium carbonate ($CaCO_3$) is an attractive option due to its high energy storage density (1790 kJ/kg), abundant supply of limestone, low cost (10 €/ton), non toxicity, and high operating temperature (near 900 °C) [8].

Using $CaCO_3$ as a TES material is reminiscent of its use in the calcium-looping (CaL) process for carbon sequestration [9]. The CaL technology utilises the carbonation reaction of calcium oxide (CaO) and the calcination reaction of $CaCO_3$ to store and reject carbon dioxide (CO_2), effectively concentrating it for carbon capture and sequestration purposes. The same concept can be applied to thermochemical energy storage due to the highly endothermic and exothermic reactions involved with CO_2 release and absorption, respectively. In CaL applications, the CaO and $CaCO_3$ powders are often moved between the calciner and carbonator reactors, while in this TES application the powers would be contained in a single packed bed reactor [10, 11]. In periods of excess energy generation, i.e. during the daytime, $CaCO_3$ absorbs thermal energy,

undergoing an endothermic reaction, and the material decomposes into CaO and CO_2 gas. This process is called calcination. During hours of energy demand, the previously stored CO_2 gas is fed back into the reactor, where the solid CaO reacts with CO_2 and dissipates heat equal to the enthalpy of the carbonation reaction. This reversible exothermic reaction is called carbonation and can be expressed by [12]:

$$CaCO_3 \leftrightarrow CaO + CO_2 \ (\Delta H_{900°C} = 165.5\ \text{kJ/mol}) \quad (1)$$

Utilising $CaCO_3$-based thermochemical reactions for heat storage has gained momentum in recent years, although Baker *et al.* [13] introduced the concept in the 1970s. Recently, process engineering studies of integrating $CaCO_3$ reactors for TES were conducted, and it was determined that the system possesses the necessary characteristics for commercial energy storage applications. Chacartegui *et al.* [14] investigated the application of CaL technology to TES in conjunction with a closed CO_2 power cycle for energy generation. When the pressure ratio of the carbonator to the turbine outlet was 3:1 and the recyclability of $CaCO_3$ was greater than 0.5 at 875 °C, the proposed model achieved a 45% of global plant efficiency. Additionally, this study discovered that the global plant efficiency can decline significantly when the reversibility of $CaCO_3$ falls below 0.2, of which it frequently does after multiple calcination/carbonation cycles [15].

Despite the favourable characteristics of $CaCO_3$, the decay in cyclic CO_2 storage capacity of the material has previously precluded it from becoming a suitable TES material. A TES system is expected to undergo thousands of absorption/desorption cycles without significant loss in energy storage capacity to become commercially viable. The storage capacity of pure $CaCO_3$ drops considerably after each carbonation/calcination reaction and reaches 25% of its initial capacity after 10 cycles and ~8% after 500 cycles [10, 16, 17]. The drop in multicyclic activity of $CaCO_3$ is due to sintering (pore-plugging) phenomena under the high temperatures used during thermochemical reactions [8, 14, 18-21].

Investigations have been conducted to improve the multicycle activity of the $CaCO_3$, with most of the focus being on reducing the sintering issue of CaO-based sorbents [8]. The addition of foreign elements (such as MgO, TiO_2, SiO_2, CuO, $CaZrO_3$) to $CaCO_3$ can cause chemical and morphological changes, limiting the particle size and controlling the microstructure of $CaCO_3$ [10, 22-33]. Wu *et al.* [34] found that a nano-sized CaO/Al_2O_3 composite showed cyclic stability of 68.3% after 50 cycles when cycling between 650 °C and 800 °C carbonation and calcination temperatures. The sintering issue was more recently addressed at 900 °C using

$CaCO_3/Al_2O_3$ composites that formed $Ca_5Al_6O_{14}$, which acted as a barrier to sintering, but also an ion conductor to promote reaction kinetics [10]. The study revealed that $CaCO_3$ doped with 20 wt% Al_2O_3 maintained cyclic stability of ~80-90% over 500 cycles. During cycling, the Ca-Al-O materials merely catalyse the sorption reactions and do not contribute to the thermodynamics of the reaction. As such, the temperatures and pressures at which the reactions occur at are not altered [10, 11, 35]. This incomparable cyclic stability addresses many issues seen in CaL studies and demonstrates great potential for TES applications.

Numerous modelling studies of high-temperature thermochemical reactors, including those using metal hydrides, metal oxides, and metal hydroxides, are already underway. However, there have been just a few numerical studies of calcium carbonate reactors for thermochemical energy storage, most of which have been conducted recently [14, 36, 37]. The lack of research on $CaCO_3$ reactors for TES applications is mostly owing to the recyclability issue associated with $CaCO_3$ material, which is unfavourable for TES applications. Recent research, however, has shown techniques for greatly enhancing $CaCO_3$'s multicyclic activity. The recent experimental and numerical studies of the carbonation process for TES have mostly used fluidised bed and rotary kiln reactors [36, 38-40]. However, the operation and numerical investigations of the carbonation reaction in fluidised or rotary kiln $CaCO_3$ reactors differ from those in the packed bed reactor used in the current work.

In the current study, initially, the reaction kinetics of ball-milled $CaCO_3/Al_2O_3$ were measured. The calculation of the reaction kinetics of the material enables the numerical investigation of the $CaCO_3/Al_2O_3$ reactor under various operating conditions. Furthermore, the kinetic model is used to conduct the numerical investigation of the packed bed reactor for TES application. The operating temperature, thermal conductivity of the composite bed, CO_2 applied pressure, and bed porosity are all parametrically analysed. This investigation provides optimisation of operating conditions for large-scale TES operating conditions.

Experimental Analysis

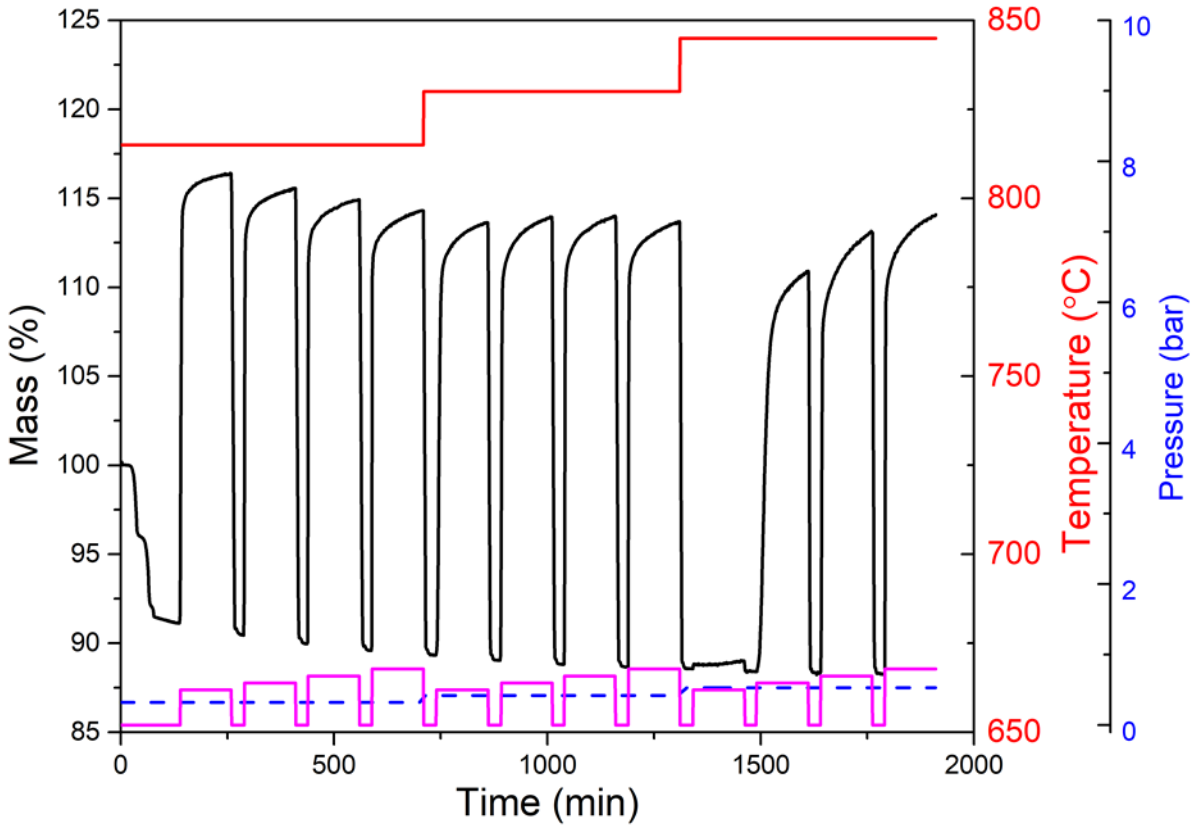

Figure 1. Reaction kinetics of $CaCO_3$ + 20 wt% Al_2O_3 data measured by TGA. Black line represents the mass loss/gain of the sample during absorption and desorption of CO_2. The red line is the isothermal temperature stages. The blue dashed line is the calculated equilibrium pressure of the material determined from thermodynamic measurements, and the purple line is the CO_2 partial pressure during the experiment. It is noted that no mass gain was measured at 845 °C and 0.5 bar CO_2 pressure as it is below the equilibrium gas pressure.

$CaCO_3$ (≥99 %, Sigma-Aldrich) was ball milled with 20 wt% Al_2O_3 (≥ 98 %, Sigma-Aldrich) and CO_2 cycled 500 times at 900 °C according to a previous study by Møller *et al.* [10]. This material was used for reaction kinetic analysis. Thermogravimetric analysis (TGA) was performed on a Netzsch (STA 449 F3 Jupiter). The sample (13.74 mg) was measured using an Al_2O_3 crucible with a lid possessing a pin-hole to allow gas exchange. The sample was cycled, starting from a semi-desorbed state, under varying CO_2 partial pressures (0.5, 0.6, 0.7, 0.8 bar) under three isothermal conditions (815, 830 and 845 °C), see Figure 1. The CO_2 partial pressures were attained by varying a mixture of Ar and CO_2 flow rates in the purge gas. In general, the program consisted of a ramp-up to 815 °C under a pure Ar flow to ensure

decomposition of the starting material. An Ar/CO_2 mixture was then flowed over the sample under isothermal conditions for 1 h, after which a pure argon flow was again passed over the sample for 30 mins to decompose the sample again. The material was then cycled under varying gas concentrations and temperatures using identical parameters. The temperature and sensitivity of the DSC were calibrated using In, Zn, Al, Ag and Au reference materials, resulting in a temperature accuracy of ± 0.2 °C, while the balance has an accuracy of ± 20 µg.

Results and Discussion

Reaction Kinetics of $CaCO_3/Al_2O_3$

The reaction kinetics of pure $CaCO_3$ were previously studied for CO_2 storage applications, where the carbonation kinetics of CaO with CO_2 were found to be a two-stage process [41-43]. The initial phase of the carbonation is a rapid and kinetically controlled surface reaction, where the later stage is relatively sluggish and controlled by the diffusion of CO_2 through the as-formed $CaCO_3$ [9]. Inconsistencies in kinetic measurements have caused discrepancies in the kinetic models due to the type of material used (e.g. limestones, calcite crystals, precipitated $CaCO_3$), experimental apparatus used for absorption/desorption measurement (e.g. thermogravimetric analysers, flow reactors), the operating conditions for carbonation/calcination reaction (temperature, pressure of CO_2) and sample size of $CaCO_3$ [44-46]. As such, a new kinetic model is required for $CaCO_3/Al_2O_3$.

It was revealed from previous investigations that the $CaCO_3$/20% Al_2O_3 composite degrades to ≈ 80-90% of the initial CO_2 storage capacity over 500 cycles and maintains the same capacity for extended cycles [10]. As such, this cycled material was used to determine the typical kinetic parameters for $CaCO_3$ during absorption of CO_2 under typical reaction conditions. It is also important to note that the capacity retention is completely a function of CO_2 pressure, temperature and time. The CO_2 pressure and temperature in the current study are different from previous work, a capacity retention of 70% is observed after 500 cycles in the current study[10]. Also, the gravimetric CO_2 storage capacity is calculated based on the 70% of capacity retention. The reaction thermodynamics of the CaO/$CaCO_3$/CO_2 system are such that the mixture will be at chemical equilibrium (no CO_2 release or absorption) at 900°C under 1 bar CO_2 pressure [12]. For absorption of CO_2 to occur under 1 bar (the pressure limits of the TGA instrument), the temperature must be below 900 °C. As such the absorption kinetics study was conducted at three different CO_2 pressures (0.6, 0.7, 0.8 bar) and temperatures (815, 830, and 845 °C). The TGA apparatus measurement shows that the carbonation reaction in $CaCO_3/Al_2O_3$ occurs

rapidly (Figure 1). The majority of the reaction (90%) was completed in less than 60 seconds, which is much faster than the previously published result of pure $CaCO_3$ carbonation reaction kinetics for TES applications [47].

The reaction rate equation for any solid-gas reaction is generally expressed as follows [48]:

$$\frac{dx}{dt} = kf(x) \tag{2}$$

where x is the reacted fraction of the solid, k is the kinetic coefficient, which is a function of temperature (T) and pressure (P), and $f(x)$ is a function determining the mechanism of the reaction, and t is the reaction time.

Using the Arrhenius equation, the kinetic coefficient, k, can be expressed as [49]

$$k = k_0 * f(P) * e^{-\frac{E_a}{RT}} \tag{3}$$

where k_o is a pre-exponential factor, $f(P)$ is a pressure-dependent term, E_a is the activation energy, and R is the universal gas constant. After separating the variables and integrating Equation 2, the integral form of the reaction rate law, ($g(x)$), is obtained.

$$g(x) = \int \frac{dx}{f(x)} = kt \tag{4}$$

Numerous kinetic functions representing chemical reactions, diffusion, nucleation, and nuclei growth mechanisms are currently available for gas-solid absorption systems [50, 51]. The volume of CO_2 absorption measured at three temperatures and pressures is fitted using known kinetic models. Model fitting approaches are based on fitting experimental data to a number of well-known solid-state reaction models listed in table 1 in order to obtain the E_a and k_o [49, 50, 52].

Table 1: Mechanism function of the various solid-gas reaction models

Model	**Differential form** ***f(x)***	**Integral form** ***g(x)***	**Exponent** ***r***
Avrami-nucleation and growth	$(1/r)(1-x)[-\ln(1-x)]^{1-r}$	$[-\ln(1-x)]^{r}$	1/4, 1/3, 2/5, 1/2, 2/3, 3/4, 1, 3/2, 2, 3, 4
Power law	$(1/r)x^{1-r}$	x^{r}	1/4, 1/3, 1/2, 1, 3/2, 2
Exponential	$(1/r)x$	$\ln x^{r}$	1, 2
Branching nucleation	$x(1-x)$	$\ln[x/(1-x)]$	
Phase boundary reaction	$(1-x)^{r}/(1-r)$	$1-(1-x)^{1-r}$	1/2, 2/3
Chemical reaction	$(1/r)(1-x)^{r}$	$1-(1-x)^{r}$	1/2, 2, 3, 4, 1/4, 1/3
1-D diffusion	$(1/2)x^{-1}$	x^{2}	
2-D diffusion	$[-\ln(1-x)]^{-1}$	$x+(1-x)\ln(1-x)$	
2-D diffusion	$(1-x)^{1/2}[1-(1-x)^{1/2}]^{-1}$	$[1-(1-x)^{1/2}]^{2}$	
2-D diffusion	$4(1-x)^{1/2}[1-(1-x)^{1/2}]^{1/2}$	$[1-(1-x)^{1/2}]^{1/2}$	
3-D diffusion	$(3/2)(1-x)^{2/3}[1-(1-x)^{1/3}]^{-1}$	$[1-(1-x)^{1/3}]^{2}$	
3-D diffusion	$(3/2)[(1-x)^{-1/3}-1]^{-1}$	$1-2x/3-(1-x)^{2/3}$	

The integral forms ($g(x)$) of the various kinetic models listed in table 1 are plotted against the time taken for the carbonation reaction at a CO_2 pressure of 0.8 bar and temperature of 845 °C as depicted in Figure 2. According to the kinetic fitting analysis, the Avrami-nucleation and growth model$[-\ln(1-x)]^{r}$ with exponent $r = 3$, provides the best linear match for the majority of carbonation processes.

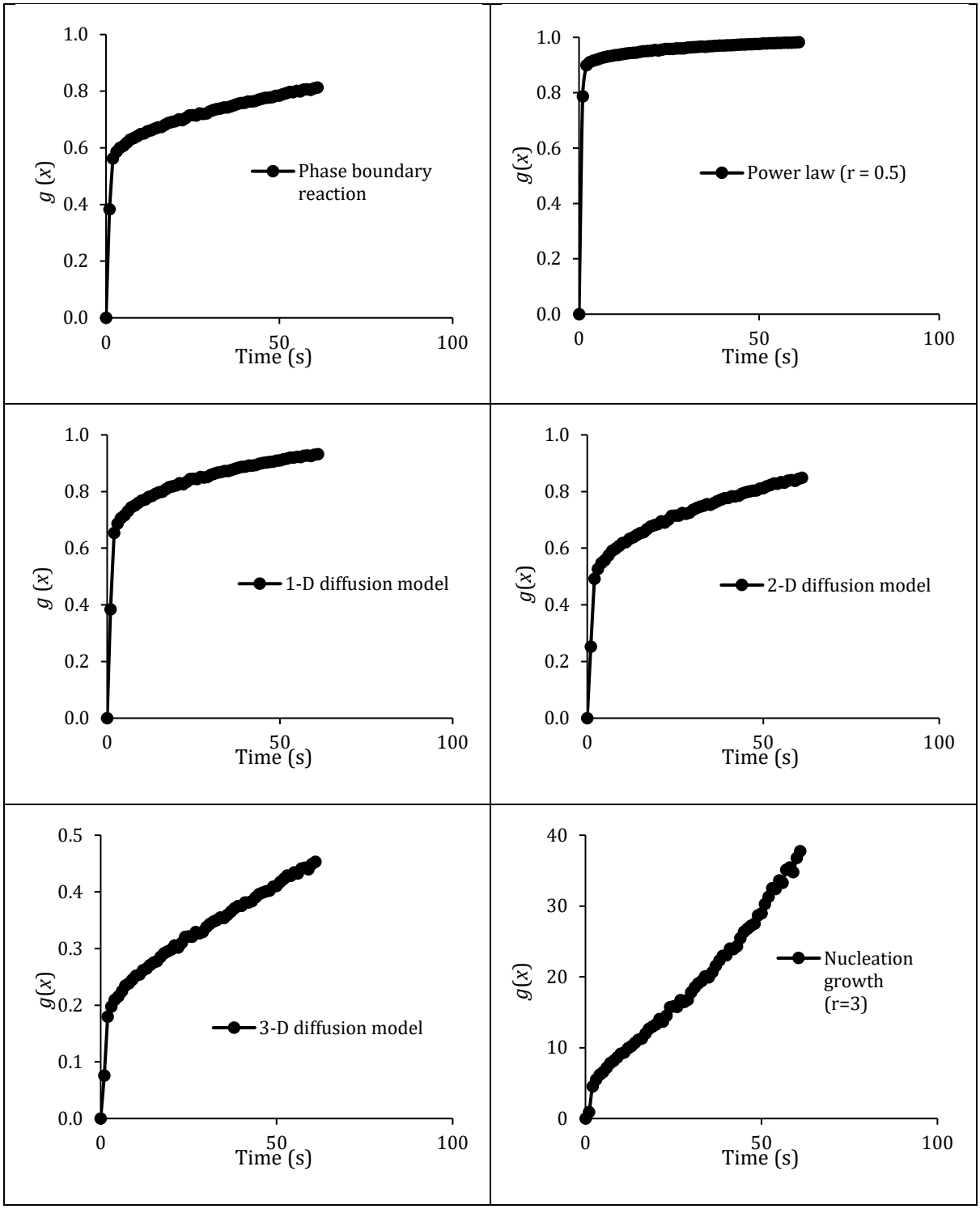

Figure 2. Comparison of the degree of fit of integral form of different kinetic models ($g(x)$) vs the time for carbonation *(t)* at 0.8 bar CO_2 pressure and temperature of 845 °C.

The effect of pressure, *f(P)* in Equation 3, on the reaction kinetics of carbonation is also investigated. Figure 3 shows that the kinetic coefficient, *k*, exhibits a linear relationship with

($(P–P_{eq})/P_{eq}$) at different temperatures. The term P_{eq} refers to the equilibrium pressure, which is determined by van't Hoff law as

$$\frac{P_{eq}}{P_{ref}} = exp^{\left(\frac{\Delta H}{RT}-\frac{\Delta S}{R}\right)} \tag{5}$$

where the reference pressure, P_{ref} = 1 bar. ΔH, ΔS, R, T are carbonation enthalpy, entropy, universal gas constant and temperature, respectively. As a result, the pressure function, $f(P)$, of the carbonation reaction is represented by

$$f(P) = \left(\frac{P - P_{eq}}{P_{eq}}\right) \tag{6}$$

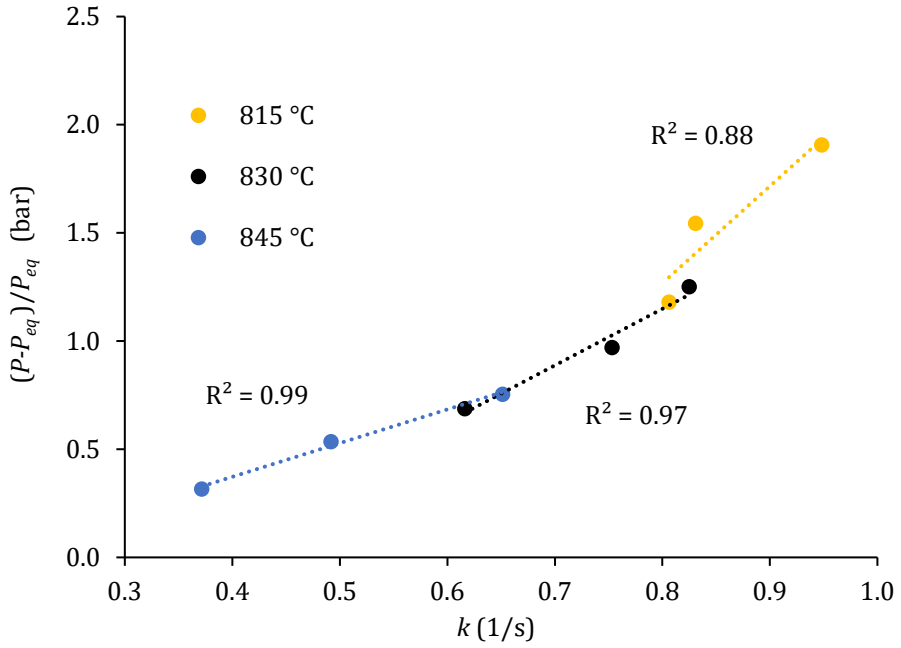

Figure 3. Plot of pressure function ($(P–P_{eq})/P_{eq}$) on the reaction vs kinetic coefficient (k) at CO_2 pressure of 0.8 bar and different temperatures.

By substituting the pressure function, $f(P)$, into equation (3) yields

$$k = k_0 * \left(\frac{P - Peq}{Peq}\right) * e^{-\frac{E_a}{RT}} \tag{7}$$

By taking the logarithm of both sides and combining with Equation 6, it can be rewritten in the form of a general equation of a line ($y = mx + c$) as

$$ln\,(k) - ln\left(\frac{P - Peq}{Peq}\right) = -\frac{Ea}{R}\frac{1}{T} + lnk_0 \tag{8}$$

Plotting (ln (k) $-ln$ (($P-P_{eq}$)/P_{eq})) against ($1/T$) for various CO_2 pressures gives a straight line with slope ($-E_a/R$) and intercept on the y axis (ln k_0). The value of activation energy (E_a) and pre-exponential factor (k_0) calculated from the slope and intercept values at CO_2 pressure of 0.6, 0.7 and 0.8 bar are listed in Table 2.

Table 2. Values of activation energy (Ea) and pre-exponential factor (k_0) of carbonation reaction at different pressures.

Pressure (bar)	E_a **(kJ/mol CO_2)**	k_0 **(s^{-1})**
0.6	215.21	1.44×10^{10}
0.7	217.61	1.52×10^{10}
0.8	219.16	1.63×10^{10}

Similarly, substituting the integral form of the kinetic model, $g(x)$, and the pressure-dependent function, $f(P)$, into Equation 4 and rearranging the terms results in the reaction rate expression as

$$\frac{dx}{dt} = k_0 * \frac{(1-x)}{3 * [-ln(1-x)]^2} * \left(\frac{P - P_{eq}}{P_{eq}}\right) * e^{\frac{-Ea}{RT}} \quad (9)$$

Numerical Analysis

Physical model of the reactor

The physical model of the $CaCO_3$ reactor considered in the present work is shown in Figure 4. A cylindrical reactor with a length and diameter of 100 mm is considered for parametric investigations. It is assumed that the bottom and top faces of the cylinder are perfectly insulated. A constant temperature boundary condition is assumed at the outer wall of the cylinder. It is analogous to a rector, with the heat transfer fluid flowing through the outer wall of the cylinder at a constant temperature. This could be accomplished by using either a high heat transfer fluid flow rate or boiling heat transfer fluid flow, the latter of which was numerically explored in our previous study [53].

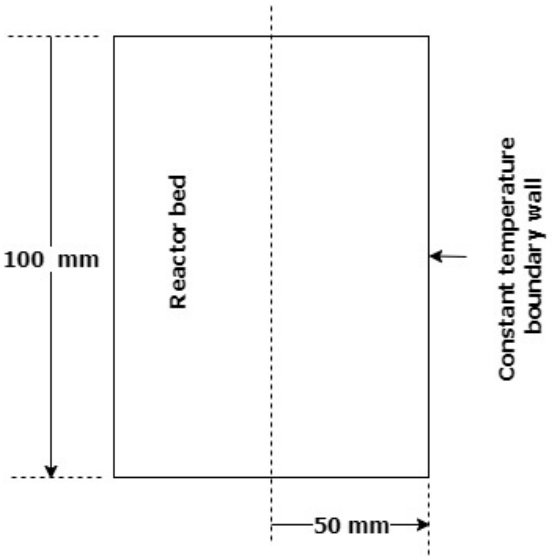

Figure 4. Schematic of the reactor bed for numerical modelling.

The following assumptions are made to simplify the simulations:

1. CO_2 is considered as an ideal gas;
2. Local thermal equilibrium is valid between CO_2 and powder particles;
3. Thermophysical properties of reactor bed are constant and homogenous;
4. CO_2 flow is neglected;
5. The volumetric expansion of the reactor bed during carbonation is neglected.

Governing Equations

The energy equation for $CaCO_3$ bed is given by [54]:

$$(\rho C_P)_e \frac{\partial T_m}{\partial t} = \nabla.(\lambda_e \nabla T_s) + \dot{Q} \tag{10}$$

where ρ is the density, C_p is specific heat, T is the temperature, t is time, λ is the thermal conductivity and $\dot{Q}$ is the heat source term which is expressed as:

$$\dot{Q} = (1-\varepsilon)\rho_s wt \frac{dx}{dt}\frac{\Delta H}{M} \tag{11}$$

where ε is the porosity of the bed, wt is the maximum mass content of CO_2, dx/dt is the reaction rate, ΔH is the enthalpy of reaction, and M is the molar mass of CO_2.

The effective volumetric heat capacity is expressed as:

$$(\rho C_P)_e = (\varepsilon \rho C_P)_{gas} + \left((1-\varepsilon)\rho C_P\right)_s \quad (12)$$

The subscript, gas, represents the gas phase, while the subscript, s, denotes the solid phase.

The effective thermal conductivity is expressed as:

$$\lambda_e = \varepsilon \lambda_g + (1-\varepsilon)\lambda_s \quad (13)$$

Table 3. Thermo-physical properties used in the numerical model [10, 55, 56]

Enthalpy of absorption (J/mol. CO_2)	ΔH	−165500
Entropy of absorption (J/K/mol. CO_2)	ΔS	−143
Density of $CaCO_3$ bed (kg/m^3)	ρ_{CaCO_3}	1850
Density of the Al_2O_3 (kg/m^3)	$\rho_{Al_2O_3}$	3800
Density of the reactor bed (80% $CaCO_3$/20% Al_2O_3) (kg/m^3)	ρ_s	2240
Specific heat capacity of $CaCO_3$ (J/kg.K)	C_{CaCO_3}	910
Specific heat capacity of Al_2O_3 (J/kg.K)	$C_{Al_2O_3}$	775
Specific heat of the reactor bed (80% $CaCO_3$/20% Al_2O_3)	C_{P_s}	883
Porosity	ε	0.66
Gravimetric CO_2 storage capacity (wt%)	wt	25
Specific heat capacity of CO_2 (J/kg.K)	C_P	1257
Molecular weight of CO_2 (kg/mol)	M	0.044
Gas constant (J/mol K)	R	8.314
Thermal conductivity of $CaCO_3$ bed (W/m.K)	λ_m	1.33

Solution procedure

The CFD modelling of the $CaCO_3$ reactor was performed using a commercial finite volume software package, ANSYS Version 2020 R1. The computational domain was generated using the Design Modeler and ANSYS Meshing used for mesh generation. The user-defined functions (UDF) have been incorporated into the CFD model to actively estimate the reaction rate of the carbonation process and equilibrium pressure. The energy equation was solved using the QUICK differencing scheme. Previously, the computational modelling of a high-

temperature thermochemical reactor for TES application was validated. The kinetic study and numerical modelling of a thermochemical reactor with helical coil heat exchanger and convective heat loss conditions were accurately simulated, and the results were found to be in good agreement with the experimental data [57].

Numerical results

Effect of CO_2 supply pressure

The influence of applied CO_2 pressure on the carbonation reaction in the reactor bed was investigated by evaluating the averaged carbonation reacted fraction, averaged bed temperature, and rate of heat absorption from the reactor. The CO_2 supply pressure of 1, 2, and 3 bar were considered for the study. A constant temperature of 815 °C was maintained at the outer wall of the reactor. The initial reacted fraction and temperature of the bed were considered as 0.01 and 815 °C, respectively.

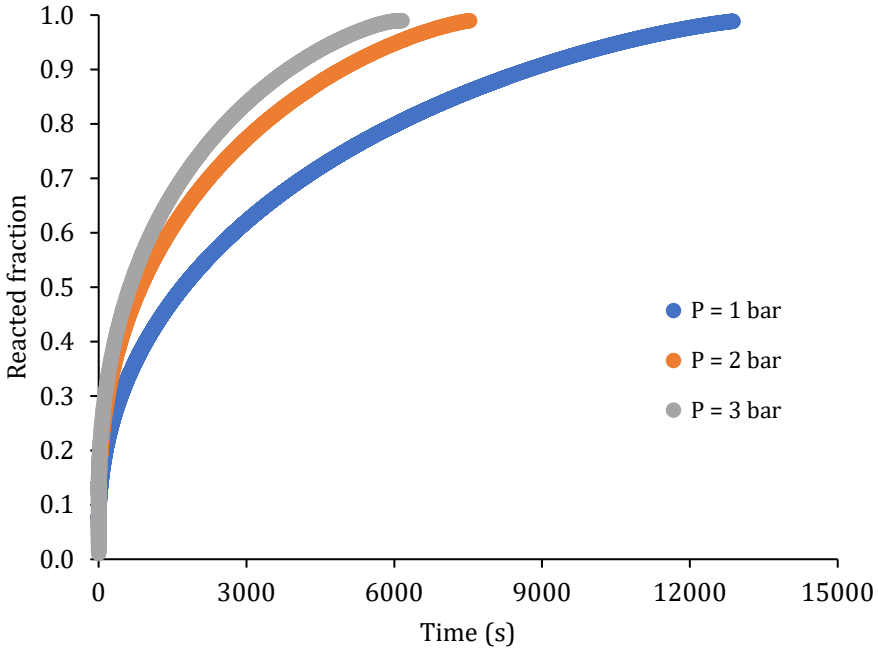

Figure 5. Effect of carbon dioxide supply pressure on average reacted fraction of $CaCO_3$ during carbonation.

Figure 5 depicts the effect of supply pressure on the averaged reacted fraction. An increase in applied pressure of CO_2 accelerates the carbonation reactions in the reactor bed. The time

required to complete the reaction is ~ 12875, ~7530, and ~6160 s when the applied CO_2 pressure of 1, 2, and 3 bar, respectively. It is discovered that increasing the applied pressure from 1 bar to 2 bar results in a 42% faster reaction but increasing the pressure from 2 bar to 3 bar results in only a 18% improvement. This variation in the performance improvement of the reactor with pressure is due to the change in kinetic parameters as the pressure increases.

Figure 6 shows the effect of applied CO_2 pressure on the temperature of the reactor bed. The bed temperature rapidly increases in the initial phase of the reaction in all three pressure scenarios. The sudden temperature rise is due to a large pressure gradient between applied pressure and equilibrium pressure. As a result, the maximum temperature of the bed reaches ~965 °C in the 3 bar scenario, while it reaches only ~887 °C under 1 bar CO_2 pressure. As the reaction progresses, the bed temperature decreases due to heat exchange to the outer wall of the reactor.

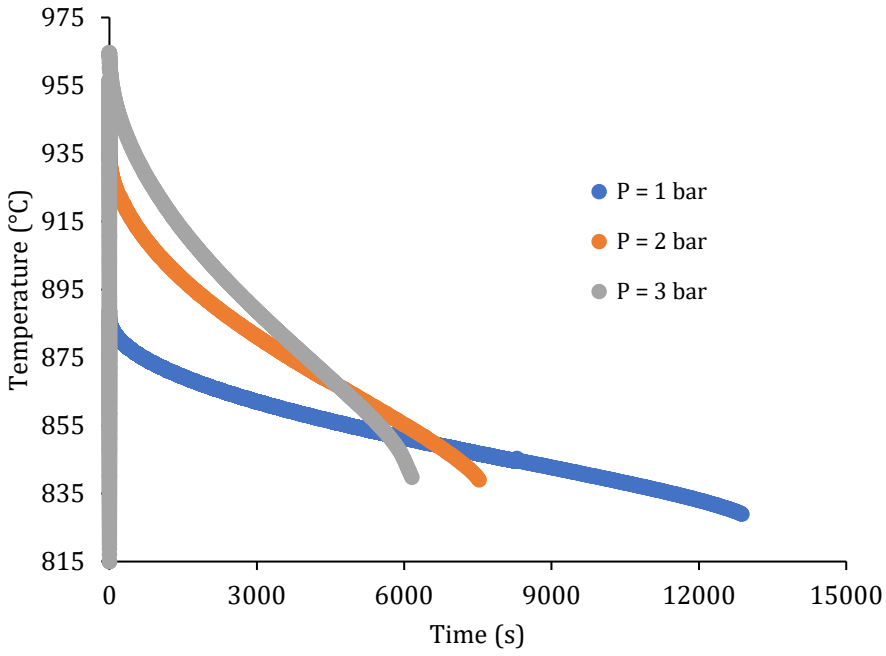

Figure 6. Effect of carbon dioxide supply pressure on temperature of the reactor bed with thermal conductivity of 1.33 W/m.K.

Figure 7 shows the variation in the heat transfer rate under varied pressures. Due to the large temperature gradient between the reactor bed and outer wall, the heat transfer rate is much higher during the initial phase of the reaction. Therefore, the maximum heat transfer rate under 3 bar CO_2 pressure exceeds 4100 W/m^2, but it is less than 2100W/m^2 under 1 bar CO_2 in the

initial reaction phase. However, as the reaction progresses, there is a significant drop in the heat transfer rate due to a drop in the temperature of the reactor bed. The heat transfer rate falls below 200 W/m^2 in all cases within 500 s of reaction.

The abrupt decrease in the heat transfer rate is caused by the characteristics of the reaction that occurs in the reactor. During the initial phase of the reaction, the reactor bed closest to the exterior wall has a faster reaction rate due to increased heat transfer to the outer wall, causing the reaction to complete more quickly. However, a large portion of the powder bed in the centre of the reactor remains unreacted. As time progresses, the fully finished reacted bed region adjacent to the reactor's outer wall restricts heat transfer from the reactor's core to the outer wall.

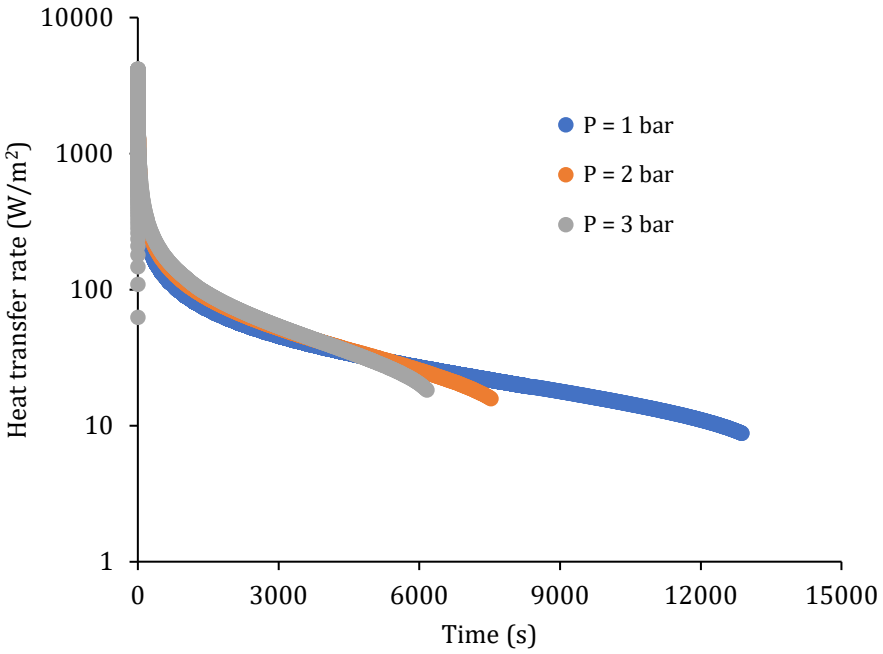

Figure 7. Effect of carbon dioxide supply pressure on heat transfer rate from the reactor bed.

Effect of thermal conductivity

A parametric investigation of thermal conductivity of the reactor bed was numerically studied using the values of 1.33, 3, and 5 W/m.K. The boundary wall temperature and initial temperature were maintained at 815 °C. A constant pressure of 1 bar CO_2 was applied for this study. Figure 8 shows that an increase in thermal conductivity has a profound effect on reactor performance. An increase in thermal conductivity of the bed from 1.33 to 5 W/m.K reduces the overall time to complete the carbonation reaction from ~12875 to ~3382 s. The improved performance due to the thermal conductivity enhancement is marginal until the reacted fraction reaches 0.2. However, as the reaction progresses, the effect propagates. The enhanced reaction rate in the later stages of the reaction in the high thermal conductivity scenario is owing to the faster heat transfer across the fully reacted reactor bed adjacent to the outer wall.

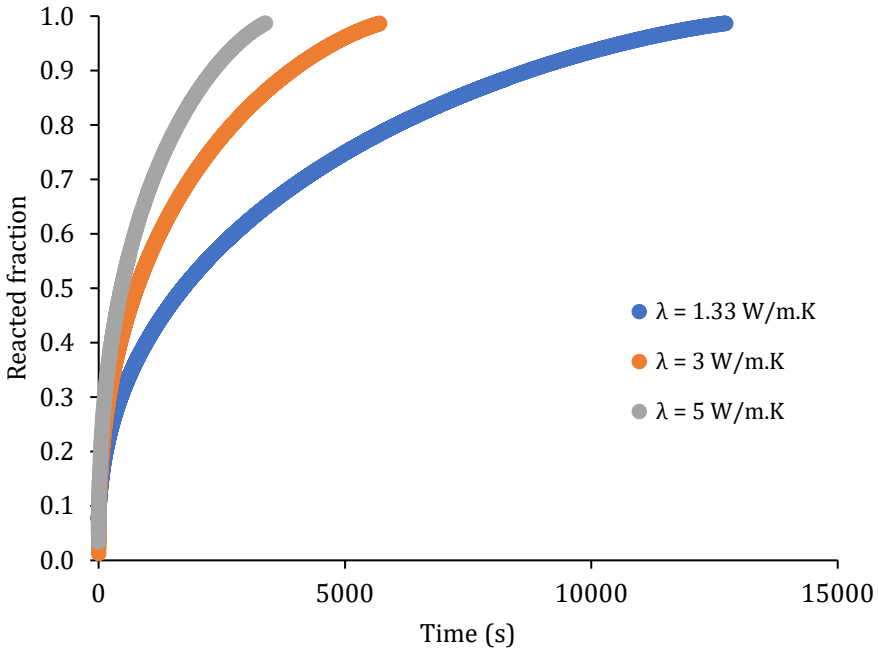

Figure 8. Effect of thermal conductivity of reactor bed on the reacted fraction at CO_2 pressure of 1 bar.

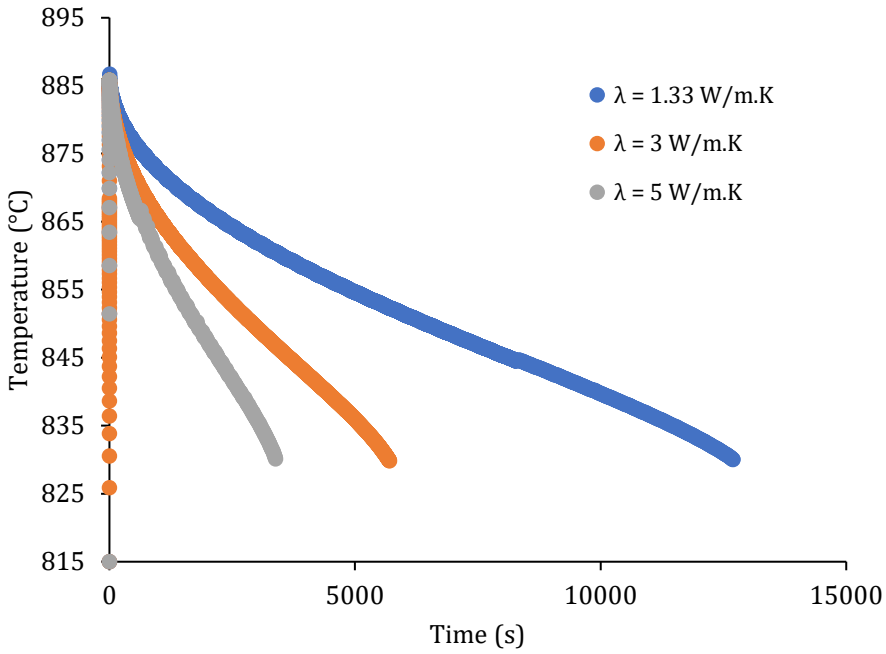

Figure 9. Effect of thermal conductivity of the bed on reactor temperature at CO_2 pressure of 1 bar.

Figure 9 shows the averaged temperature of the reactor bed at various thermal conductivity values. It can be seen from the plot that the thermal conductivity augmentation has a negligible effect on the maximum temperature of the reactor bed. The maximum temperature of the reactor bed reaches ~ 886°C for all cases resulting in a similar performance of the reactor in the initial phase of the reaction. The bed with a higher thermal conductivity cools down faster as the reaction progresses due to more effective heat exchange to the outer wall of the reactor bed. As such, for a thermal conductivity of 5 W/m.K it takes 3382 s for the bed temperature to reach 830 °C, while it requires 12615 s for a thermal conductivity of 1.33 W/m.K.

The influence of thermal conductivity on the heat transfer rate is depicted in Figure 10. Unlike the average temperature profile of the reactor bed, the total heat transfer rate is much higher when thermal conductivity is increased. For example, the maximum heat transfer rate reaches ~7565 W/m^2 in the 5 W/m.K case, whereas it reaches ~2050 W/m^2 when thermal conductivity is 1.33 W/m.K. Furthermore, the elevated heat transfer rate is only visible for a few seconds before dropping below 610 W/m^2 in all scenarios within 100 seconds.

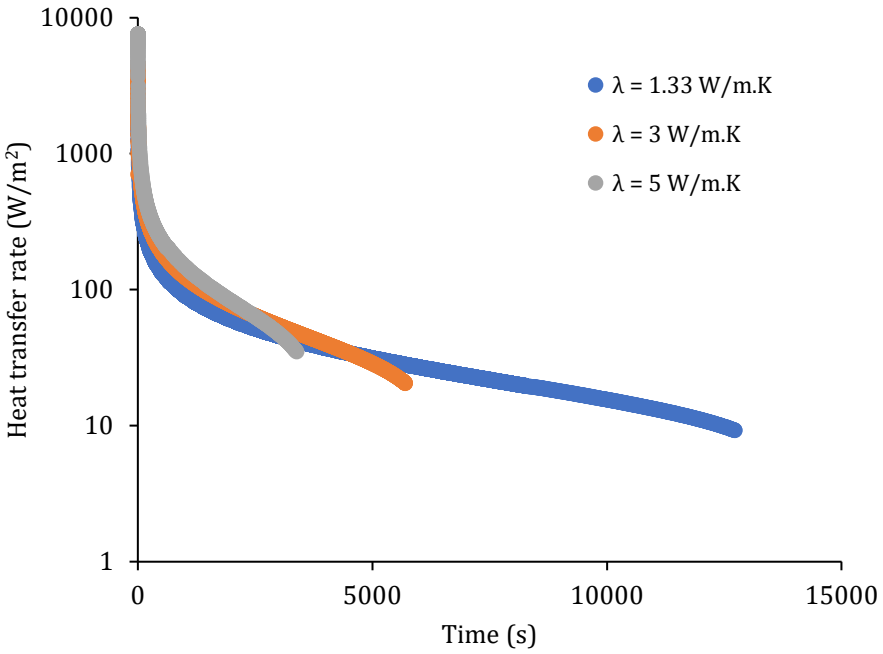

Figure 10. Effect of thermal conductivity of bed on heat transfer rate at CO_2 pressure of 1 bar.

Boundary temperature

The influence of boundary temperature of the reactor bed was investigated by maintaining boundary temperatures of 815, 830, 845 °C under constant CO_2 pressure of 1 bar. The effect of the boundary wall temperature on the reactor performance is depicted in Figure 11. The rise in the boundary temperature increases the time required to complete the carbonation reaction. This effect is minor until the reacted fraction reaches 0.3 but becomes more noticeable as the reaction process. The time taken to complete the reaction is ~12875, ~16415, ~22520 s, when the boundary temperatures are 815, 830, 845 °C, respectively. Therefore, a decrease in wall temperature by 30 °C decreases the reaction completion time by ~43%. Increased heat transfer from the reactor bed results in a faster reaction at low-temperature boundary conditions. The higher heat transfer from the reactor bed contributes to a faster reaction in the low-temperature boundary cases.

The temperature variation of the exterior wall of the reactor can be interpreted as the temperature of the heat transfer fluid flowing through the real-world application. When a single-phase heat transfer fluid flow is supplied to the reactor's outer wall, the results indicate how increasing the temperature of the heat transfer fluid as it passes through the reactor affects reactor performance.

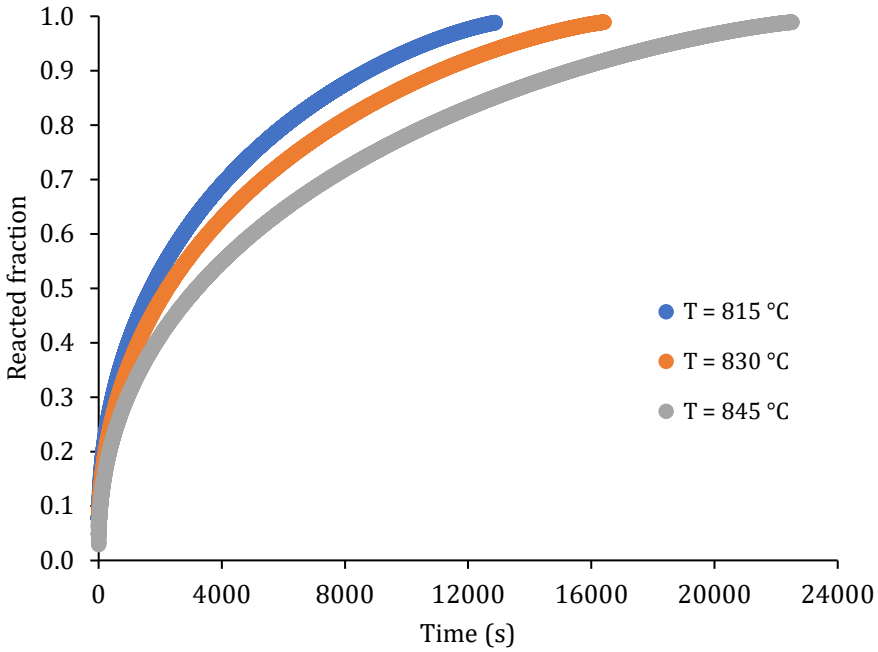

Figure 11. Effect of reactor's boundary temperature on the reacted fraction at CO_2 pressure of 1 bar.

Figure 12 shows the temperature variation of the reacted fraction at different boundary wall temperatures. Similar to the previous parametric investigations in this study, the temperature of the bed rises rapidly in the initial few seconds. The study suggests that the boundary temperature does not effectively influence the maximum temperature of the bed, as for all cases the highest temperature of the bed reaches ~886 °C within a few seconds of reaction initiation. Due to faster heat exchange to the outer wall of the reactor, the temperature of the bed drops faster when the boundary wall is at a minimum (815 °C).

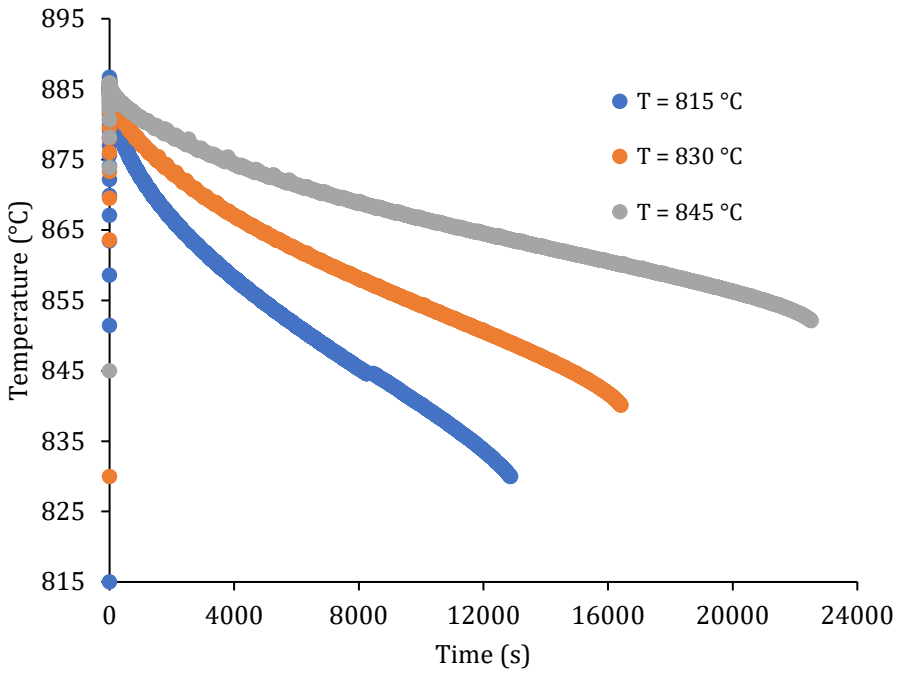

Figure 12. Effect of boundary temperature of the reactor temperature at CO_2 pressure of 1 bar.

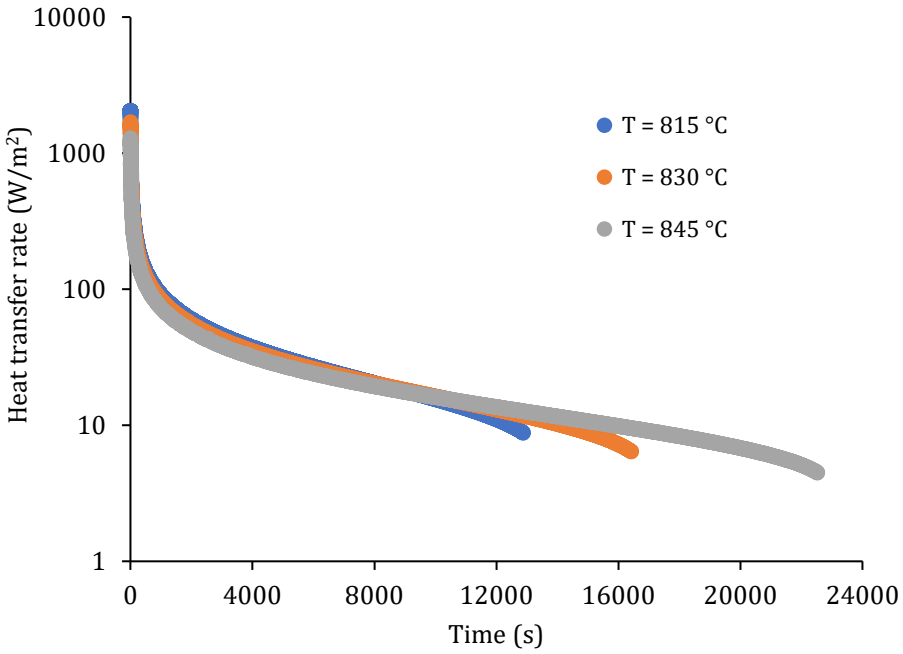

Figure 13. Effect of boundary temperature on the heat transfer rate at CO_2 pressure of 1 bar.

Figure 13 illustrates the impact of the boundary temperature of the reactor on the heat transfer rate from the reactor. The heat transfer rate is highest when the temperature is 815 °C due to the more significant temperature gradient between the reactor bed and outer wall. The maximum heat transfer rate is ~2050, ~1695 and ~1294 W/m^2 when the boundary temperature is 815, 830, 845 °C, respectively. For all scenarios, the higher heat transfer rate is observed only in the initial phase of the reaction before quickly dropping to below 470 W/m^2 within 50 s.

Study of calcium carbonate reactor with graphite fin

Previous research has demonstrated that integrating an extended surface fin into a thermochemical reactor improves the reactor's heat transfer rate and performance. Therefore, a study was carried out to ascertain whether improved performance of a carbonate TES reactor would be improved with a graphite fin inserted into the centre of the reactor, as illustrated in Figure 14. To compare the performance of the reactor with and without the fin, the reactor bed thickness and height were kept constant at 100 mm (see Figure 4). The graphite fin has an outside diameter of 15.9 mm (5/8 inch) and a total length of 200 mm, of which 100 mm extends beyond the reactor bed. The thermophysical properties of the graphite fin provided by Toyo Tanso Co.Ltd were used in this investigation [58].

A constant boundary temperature of 800 °C was applied at the outer wall of the reactor bed. The extended graphite fin was assumed to undergo natural convective heat loss to the ambient. The ambient temperature was set to 25 °C, and a heat transfer coefficient of 10 W/m^2.K (average value for natural convection for a vertical fin) was assumed. The initial temperature of both the reactor bed and the graphite fin was 800 °C, while a constant CO_2 supply pressure of 1 bar was applied. The investigations were performed under assumed thermal conductivity conditions of 1.33 and 5 W/m.K for the carbonate bed.

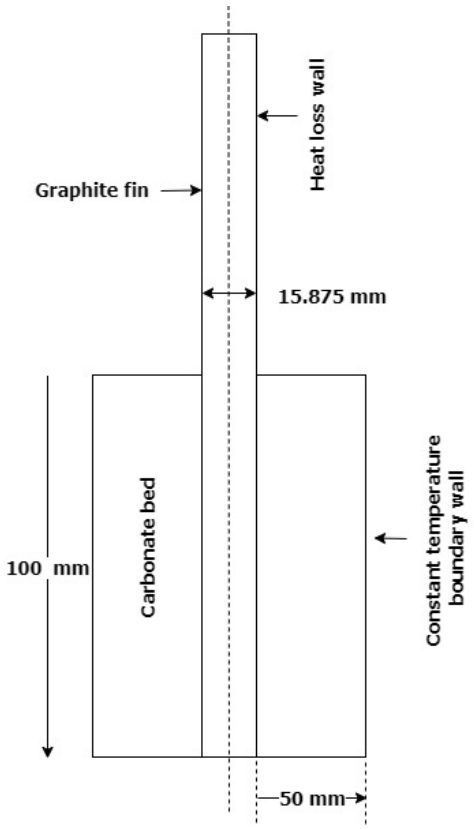

Figure 14. Schematic of carbonate reactor bed with graphite fin for numerical modelling.

Figures 15 and 16 depict the contours of temperature and reacted fraction in the reactor bed over time intervals of 100, 500, 1000, and 2000 s. The temperature contour plots demonstrate that during the initial stages of the reaction, the temperature inside the reactor bed approaches ~ 900 °C for the two thermal conductivity values. The temperature of the reactor decreases over time as a result of heat absorption from the reactor bed. Due to the increased heat transfer, a faster temperature drops occur in the 5 W/m.K case than in the 1.33 W/m.K case. As a result, in the 5 W/m.K scenario, the carbonation process advances more rapidly. The reacted fraction contour indicates that most reactor materials are carbonated at 2000 s when the thermal conductivity of the bed was 5 W/m.K, whereas a significant amount of materials remain unreacted at 1.33 W/m.K. In addition, the reacted fraction contour demonstrates that the material at the outer boundary of the reactor and near the graphite fin carbonates more rapidly at higher thermal conductivity values. This is because these locations experience a significantly increased heat transfer coefficient, as such the reaction rate is increased when the thermal conductivity is higher.

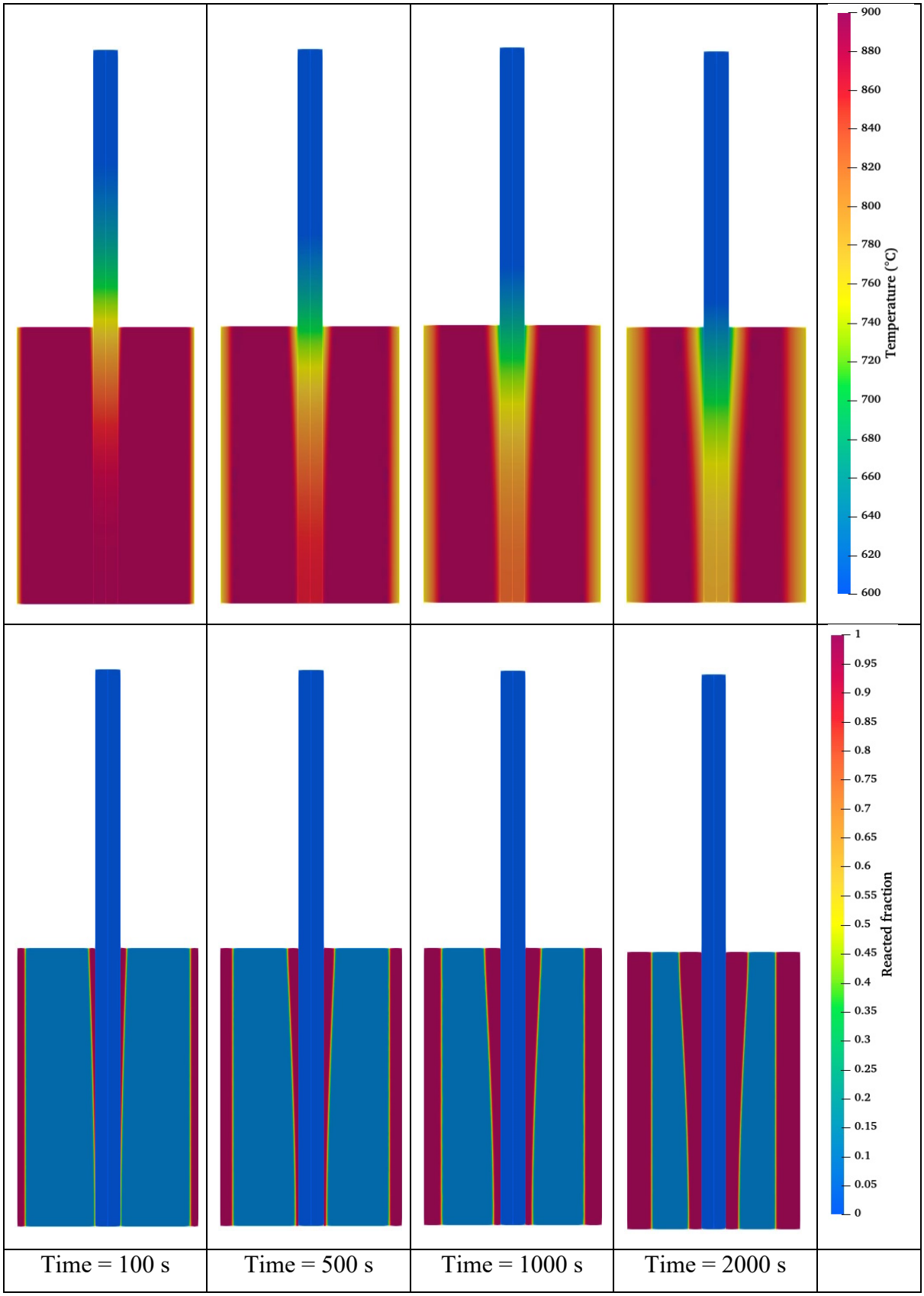

Figure 15. Distribution of the reactor's temperature (top rows) and reacted fraction (bottom rows) at various time intervals at a thermal conductivity of 1.33 W/m.K.

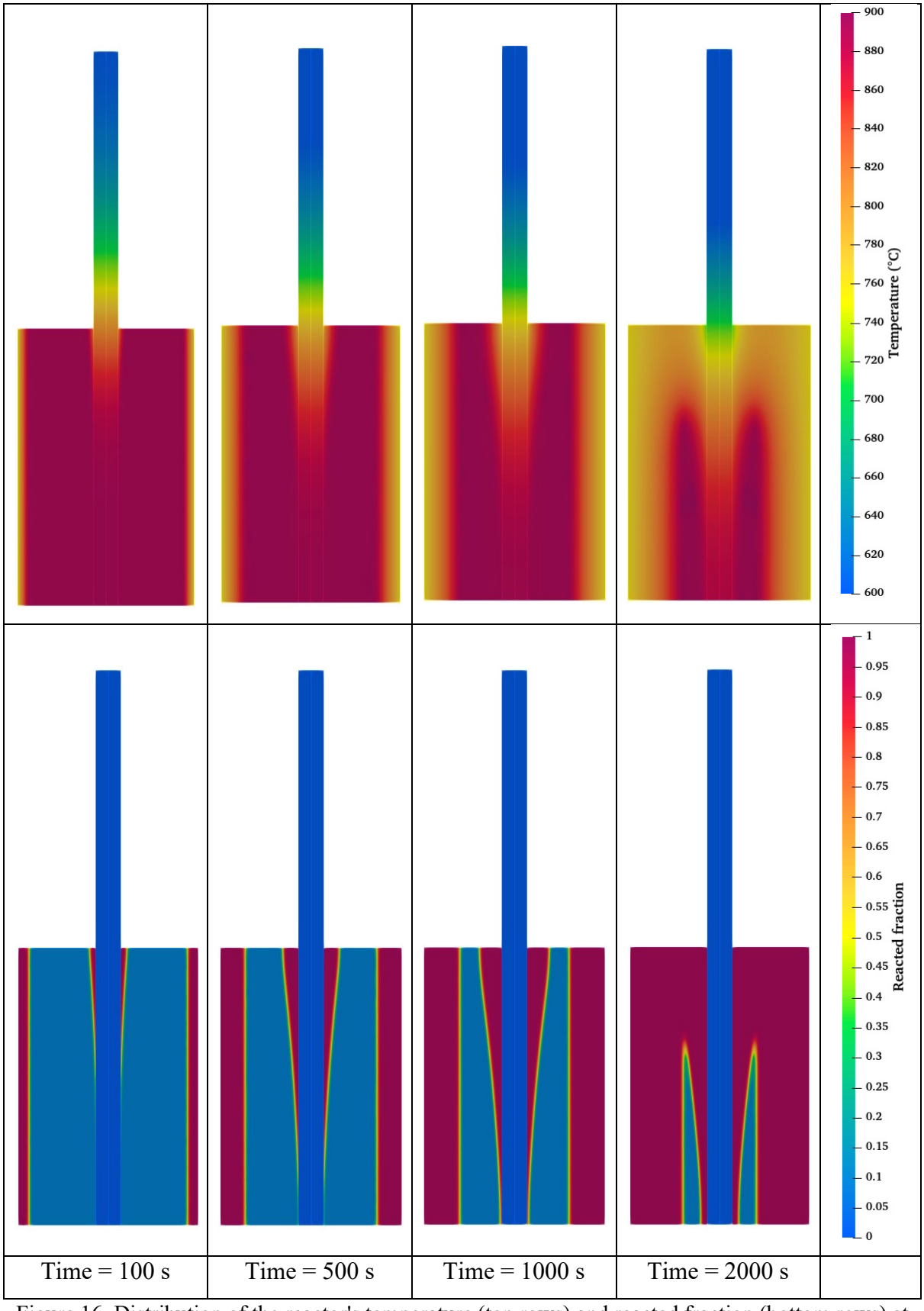

Figure 16. Distribution of the reactor's temperature (top rows) and reacted fraction (bottom rows) at various time intervals at a thermal conductivity of 5 W/m.K.

Figure 17 compares the averaged reacted fraction of the reactor with and without a fin at the two thermal conductivity values studied. With a thermal conductivity of 1.33 /m.K, it is evident that the scenario with the graphite fin shows that the reactor bed has greatly enhanced performance. The reacted fraction remains identical among the both designs until it reaches 0.4, at which point the carbonation reaction accelerates in the reactor with the fin and the reaction takes ~5910 s to complete, whereas the process extends and completes at ~10580 s in a rector without a fin. Interestingly, using a graphite fin when the thermal conductivity of the bed is 5 W/m.K has negligible effect on the reactor's performance.

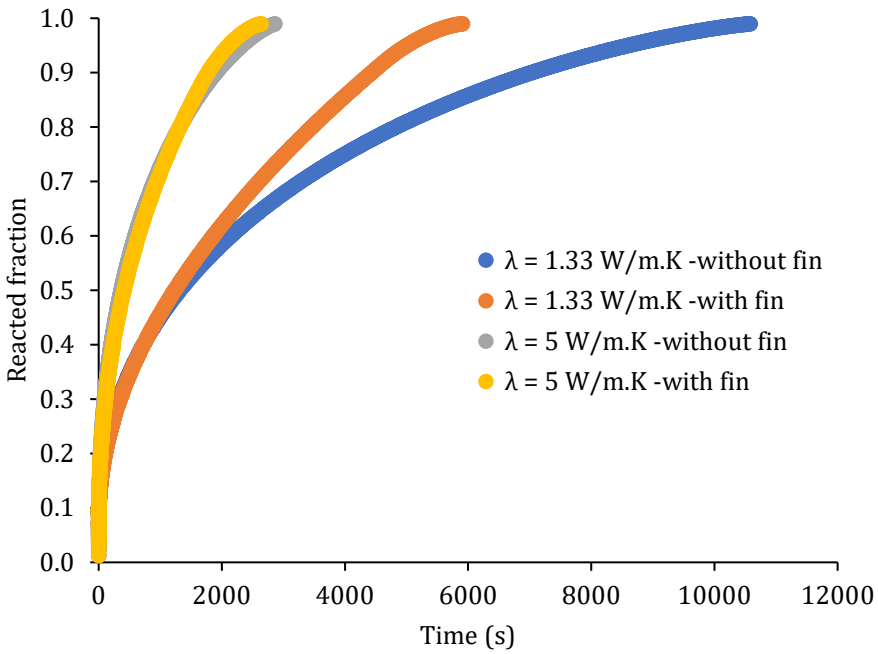

Figure 17 Comparison of averaged reacted fraction of reactor with and without the graphite fin at a thermal conductivity of 1.33 and 5 W/m.K.

The absence of increased performance under higher thermal conductivity conditions is due to the reduced rate of heat transfer across the extended fins surface. The heat is transferred from the reactor bed in two ways: through the outer wall of the reactor and the extended graphite fin. Among these two methods, the major share of heat energy is removed from the reactor bed through the outer wall of the reactor. As the thermal conductivity of the reactor bed increases, the amount of heat energy transferred through the outer wall increases and the percentage of heat energy transferred through the outer wall further increases (or reduces the percentage of heat transfer through the extended fin). Additionally, due to the higher level of heat transport,

the reaction is finished significantly faster in the high thermal conductivity condition. In contrast, the reaction takes a long time to complete in the low thermal conductivity case and a considerable amount of heat energy is transferred through the fin. This results in improved performance in the 1.33 W/m.K scenario and negligible performance gain in the 5 W/m. K case.

The results from this study emphasise the ability to have enhanced performance in future $CaCO_3$ TES reactors. Performance can be improved by raising the thermal conductivity of the powder bed and/or increasing the heat transfer area by introducing an extended fin into the reactor. Both of these strategies, however, add complexity to the reactor's construction and incur additional costs. Furthermore, once the thermal conductivity of the bed is increased the addition of the fin may not improve the reactor's performance any further. Overall, these additional changes to the reactor architecture may not be required if fast discharge of the battery is not required and energy is required at a slow but steady rate.

Conclusions

A mixture of $CaCO_3$ + 20 wt% Al_2O_3 has previously been shown to be a potential thermal energy storage material due to its operating temperature and ability to reversibly absorb CO_2 over more than 500 cycles. To date, numerical studies on this system have not been undertaken due to the requirement to determine the kinetic model for the CO_2 absorption process. TGA was used to measure the data and a kinetic model was obtained, and a numerical investigation of the cylindrical $CaCO_3$ reactor was conducted. The supply pressure of CO_2, the reactor bed's thermal conductivity, and the reactor wall's boundary temperature were considered for the parametric investigations. The conclusions can be drawn as follows:

- The kinetic study reveals that the carbonation reaction in the $CaCO_3/Al_2O_3$ takes place rapidly. The carbonation reaction follows the Avrami nucleation growth model with an exponent 3 reaction model.
- The time to complete the reaction reduces by ~ 42% when the applied pressure increases from 1 to 2 bar CO_2. However, as the applied pressure increases from 2 to 3 bar CO_2, only a 18% reduction in the time to complete the reaction is visible. The maximum temperature of the reactor bed increases from ~ 887 to ~ 965 °C when the applied CO_2 pressure rises from 1 to 3 bar.

- The carbonation reaction is ~ 74% faster when the thermal conductivity of the bed increases from 1.33 to 5 W/m.K. The maximum temperature of the reactor is independent of the thermal conductivity of the bed and the wall temperature of the reactor.
- A 43% performance improvement is shown in the reactor when the boundary wall temperature is reduced by 30 °C.
- The carbonation reaction is enhanced by ~ 44% when a graphite fin is added to a reactor with thermal conductivity of 1.33 W/m.K is, while the effect of adding a graphite fin to a reactor with thermal conductivity of 5 W/m.K is negligible.

Declaration of competing interest

The authors declare that they have no known competing financial interests or personal relationships that could have appeared to influence the work reported in this paper.

Acknowledgements

CEB, TC, TDH and AM acknowledge the financial support of the Australian Research Council (ARC) for Linkage Project LP150100730 and DP200102301. CEB, MP and TDH acknowledge the financial support of the Global Innovation Linkage grant (GIL73589). MP also acknowledges the ARC for Future Fellowship FT160100303. This work was supported by resources provided by the Pawsey Supercomputing Centre with funding from the Australian Government and the Government of Western Australia.

References

[1] Gil A, Medrano M, Martorell I, Lázaro A, Dolado P, Zalba B, et al. State of the art on high temperature thermal energy storage for power generation. Part 1—Concepts, materials and modellization. Renewable and Sustainable Energy Reviews. 2010;14:31-55.
[2] Wagner SJ, Rubin ES. Economic implications of thermal energy storage for concentrated solar thermal power. Renewable Energy. 2014;61:81-95.
[3] Pardo P, Deydier A, Anxionnaz-Minvielle Z, Rougé S, Cabassud M, Cognet P. A review on high temperature thermochemical heat energy storage. Renewable and Sustainable Energy Reviews. 2014;32:591-610.
[4] N'Tsoukpoe KE, Liu H, Le Pierrès N, Luo L. A review on long-term sorption solar energy storage. Renewable and Sustainable Energy Reviews. 2009;13:2385-96.
[5] Poupin L, Humphries TD, Paskevicius M, Buckley CE. A thermal energy storage prototype using sodium magnesium hydride. Sustain Energy Fuels. 2019;3:985-95.

[6] Urbanczyk R, Peinecke K, Peil S, Felderhoff M. Development of a heat storage demonstration unit on the basis of Mg_2FeH_6 as heat storage material and molten salt as heat transfer media. Int J Hydrogen Energy. 2017;42:13818-26.
[7] Carrillo AJ, González-Aguilar J, Romero M, Coronado JM. Solar Energy on Demand: A Review on High Temperature Thermochemical Heat Storage Systems and Materials. Chem Rev. 2019;119:4777-816.
[8] Benitez-Guerrero M, Sarrion B, Perejon A, Sanchez-Jimenez PE, Perez-Maqueda LA, Manuel Valverde J. Large-scale high-temperature solar energy storage using natural minerals. Solar Energy Materials and Solar Cells. 2017;168:14-21.
[9] Butler JW, Grace JR. 16 - High-pressure systems and processes for calcium looping. In: Fennell P, Anthony B, editors. Calcium and Chemical Looping Technology for Power Generation and Carbon Dioxide (CO2) Capture: Woodhead Publishing; 2015. p. 377-408.
[10] Møller KT, Ibrahim A, Buckley CE, Paskevicius M. Inexpensive thermochemical energy storage utilising additive enhanced limestone. Journal of Materials Chemistry A. 2020;8:9646-53.
[11] Møller KT, Humphries TD, Berger A, Paskevicius M, Buckley CE. Thermochemical energy storage system development utilising limestone. Chemical Engineering Journal Advances. 2021;8:100168.
[12] Outukumpu, HSC Chemistry, Houston, version 6.
[13] Barker R. The reactivity of calcium oxide towards carbon dioxide and its use for energy storage. Journal of Applied Chemistry and Biotechnology. 1974;24:221-7.
[14] Chacartegui R, Alovisio A, Ortiz C, Valverde JM, Verda V, Becerra JA. Thermochemical energy storage of concentrated solar power by integration of the calcium looping process and a CO2 power cycle. Applied Energy. 2016;173:589-605.
[15] Alovisio A, Chacartegui R, Ortiz C, Valverde JM, Verda V. Optimizing the CSP-Calcium Looping integration for Thermochemical Energy Storage. Energy Conversion and Management. 2017;136:85-98.
[16] Stanmore BR, Gilot P. Review—calcination and carbonation of limestone during thermal cycling for CO2 sequestration. Fuel Processing Technology. 2005;86:1707-43.
[17] Sun P, Grace JR, Lim CJ, Anthony EJ. The effect of CaO sintering on cyclic CO2 capture in energy systems. AIChE Journal. 2007;53:2432-42.
[18] Grasa GS, Abanades JC, Alonso M, González B. Reactivity of highly cycled particles of CaO in a carbonation/calcination loop. Chemical Engineering Journal. 2008;137:561-7.
[19] Grasa G, Murillo R, Alonso M, Abanades JC. Application of the random pore model to the carbonation cyclic reaction. AIChE Journal. 2009;55:1246-55.
[20] Valverde JM, Sanchez-Jimenez PE, Perez-Maqueda LA. Limestone Calcination Nearby Equilibrium: Kinetics, CaO Crystal Structure, Sintering and Reactivity. The Journal of Physical Chemistry C. 2015;119:1623-41.
[21] Benitez-Guerrero M, Valverde JM, Sanchez-Jimenez PE, Perejon A, Perez-Maqueda LA. Multicycle activity of natural CaCO3 minerals for thermochemical energy storage in Concentrated Solar Power plants. Solar Energy. 2017;153:188-99.
[22] Zhu Q, Zeng S, Yu Y. A Model to Stabilize CO2 Uptake Capacity during Carbonation–Calcination Cycles and its Case of CaO–MgO. Environmental Science & Technology. 2017;51:552-9.
[23] Filitz R, Kierzkowska AM, Broda M, Müller CR. Highly Efficient CO2 Sorbents: Development of Synthetic, Calcium-Rich Dolomites. Environmental Science & Technology. 2012;46:559-65.
[24] Li L, King DL, Nie Z, Howard C. Magnesia-Stabilized Calcium Oxide Absorbents with Improved Durability for High Temperature CO2 Capture. Industrial & Engineering Chemistry Research. 2009;48:10604-13.
[25] Park J, Yi KB. Effects of preparation method on cyclic stability and CO2 absorption capacity of synthetic CaO–MgO absorbent for sorption-enhanced hydrogen production. International Journal of Hydrogen Energy. 2012;37:95-102.
[26] Da Y, Xuan Y, Teng L, Zhang K, Liu X, Ding Y. Calcium-based composites for direct solar-thermal conversion and thermochemical energy storage. Chemical Engineering Journal. 2020;382:122815.

[27] Yang L, Huang Z, Huang G. Fe- and Mn-Doped Ca-Based Materials for Thermochemical Energy Storage Systems. Energy & Fuels. 2020;34:11479-88.
[28] Valverde JM, Perejon A, Perez-Maqueda LA. Enhancement of Fast CO2 Capture by a Nano-SiO2/CaO Composite at Ca-Looping Conditions. Environmental Science & Technology. 2012;46:6401-8.
[29] Manovic V, Anthony EJ. Integration of Calcium and Chemical Looping Combustion using Composite CaO/CuO-Based Materials. Environmental Science & Technology. 2011;45:10750-6.
[30] Wang Y, Zhu Y, Wu S. A new nano CaO-based CO2 adsorbent prepared using an adsorption phase technique. Chemical Engineering Journal. 2013;218:39-45.
[31] Zhang L, Lu Y, Rostam-Abadi M. Sintering of calcium oxide (CaO) during CO2 chemisorption: a reactive molecular dynamics study. Physical Chemistry Chemical Physics. 2012;14:16633-43.
[32] Koirala R, Gunugunuri KR, Pratsinis SE, Smirniotis PG. Effect of Zirconia Doping on the Structure and Stability of CaO-Based Sorbents for CO2 Capture during Extended Operating Cycles. The Journal of Physical Chemistry C. 2011;115:24804-12.
[33] Tregambi C, Salatino P, Solimene R, Montagnaro F. An experimental characterization of Calcium Looping integrated with concentrated solar power. Chemical Engineering Journal. 2018;331:794-802.
[34] Wu SF, Li QH, Kim JN, Yi KB. Properties of a Nano CaO/Al2O3 CO2 Sorbent. Industrial & Engineering Chemistry Research. 2008;47:180-4.
[35] Møller KT, Berger A, Paskevicius M, Buckley CE. Synergetic effect of multicomponent additives on limestone when assessed as a thermochemical energy storage material. J Alloys Compd. 2022;891:161954.
[36] Ortiz C, Chacartegui R, Valverde JM, Alovisio A, Becerra JA. Power cycles integration in concentrated solar power plants with energy storage based on calcium looping. Energy Conversion and Management. 2017;149:815-29.
[37] Tesio U, Guelpa E, Verda V. Integration of thermochemical energy storage in concentrated solar power. Part 1: Energy and economic analysis/optimization. Energy Conversion and Management: X. 2020;6:100039.
[38] Tregambi C, Montagnaro F, Salatino P, Solimene R. Directly irradiated fluidized bed reactors for thermochemical processing and energy storage: Application to calcium looping. AIP Conference Proceedings. 2017;1850:090007.
[39] Tescari S, Neises M, de Oliveira L, Roeb M, Sattler C, Neveu P. Thermal model for the optimization of a solar rotary kiln to be used as high temperature thermochemical reactor. Solar Energy. 2013;95:279-89.
[40] Shimizu T, Hirama T, Hosoda H, Kitano K, Inagaki M, Tejima K. A Twin Fluid-Bed Reactor for Removal of CO2 from Combustion Processes. Chemical Engineering Research and Design. 1999;77:62-8.
[41] Bhatia SK, Perlmutter DD. Effect of the product layer on the kinetics of the CO2-lime reaction. AIChE Journal. 1983;29:79-86.
[42] Mess D, Sarofim AF, Longwell JP. Product Layer Diffusion during the Reaction of Calcium Oxide with Carbon Dioxide. Energy & Fuels. 1999;13:999-1005.
[43] Silaban A, Harrison DP. HIGH TEMPERATURE CAPTURE OF CARBON DIOXIDE: CHARACTERISTICS OF THE REVERSIBLE REACTION BETWEEN CaO(s) and CO2(g). Chemical Engineering Communications. 1995;137:177-90.
[44] Sun P, Grace JR, Lim CJ, Anthony EJ. Determination of intrinsic rate constants of the CaO–CO2 reaction. Chemical Engineering Science. 2008;63:47-56.
[45] Scaltsoyiannes A, Lemonidou A. CaCO3 decomposition for calcium-looping applications: Kinetic modeling in a fixed-bed reactor. Chemical Engineering Science: X. 2020;8:100071.
[46] Wang H, Li Z, Li Y, Cai N. Reduced-order model for CaO carbonation kinetics measured using micro-fluidized bed thermogravimetric analysis. Chemical Engineering Science. 2021;229:116039.

[47] Ortiz C, Valverde JM, Chacartegui R, Perez-Maqueda LA. Carbonation of Limestone Derived CaO for Thermochemical Energy Storage: From Kinetics to Process Integration in Concentrating Solar Plants. ACS Sustainable Chemistry & Engineering. 2018;6:6404-17.
[48] Khawam A, Flanagan DR. Solid-State Kinetic Models: Basics and Mathematical Fundamentals. The Journal of Physical Chemistry B. 2006;110:17315-28.
[49] Vyazovkin S, Burnham AK, Criado JM, Pérez-Maqueda LA, Popescu C, Sbirrazzuoli N. ICTAC Kinetics Committee recommendations for performing kinetic computations on thermal analysis data. Thermochimica Acta. 2011;520:1-19.
[50] Li Q, Chou K-C, Lin Q, Jiang L-J, Zhan F. Hydrogen absorption and desorption kinetics of Ag–Mg–Ni alloys. International Journal of Hydrogen Energy. 2004;29:843-9.
[51] Fedunik-Hofman L, Bayon A, Donne SW. Kinetics of Solid-Gas Reactions and Their Application to Carbonate Looping Systems. Energies. 2019;12:2981.
[52] Fedunik-Hofman L, Bayon A, Donne SW. Comparative Kinetic Analysis of CaCO3/CaO Reaction System for Energy Storage and Carbon Capture. Applied Sciences. 2019;9.
[53] Mathew A, Nadim N, Chandratilleke TT, Humphries TD, Buckley CE. Investigation of boiling heat transfer for improved performance of metal hydride thermal energy storage. International Journal of Hydrogen Energy. 2021;46:28200-13.
[54] Ansys® Academic Research Mechanical R, Help System, ANSYS-FLUENT Theory Guide, ANSYS, Inc.
[55] Lemmon EW, McLinden MO, Friend DG, National Institute of S, Technology. Thermophysical properties of fluid systems. 1998.
[56] Touloukian YS. Thermal Expansion: Nonmetallic Solids, Thermophysical Properties of Matter. 1977.
[57] Mathew A, Nadim N, Chandratilleke TT, Humphries TD, Paskevicius M, Buckley CE. Performance analysis of a high-temperature magnesium hydride reactor tank with a helical coil heat exchanger for thermal storage. Int J Hydrogen Energy. 2021;46:1038-55.
[58] Catalog. https://www.toyotanso.com/Products/catalogenfullpdf20.